Polyhedron 27 (2008) 1917–1924

Contents lists available at ScienceDirect

Polyhedron

journal homepage: www.elsevier.com/locate/poly

New Ru(II)–dmso complexes with heterocyclic hydrazone ligands towards cancer chemotherapy

Viswanathan Mahalingam [a], Nataraj Chitrapriya [a], Frank R. Fronczek [b], Karuppannan Natarajan [a,*]

[a] Department of Chemistry, Bharathiar University, Coimbatore 641 046, India
[b] Department of Chemistry, Louisiana State University, Baton Rouge, LA 70803, USA

ARTICLE INFO

Article history:
Received 28 August 2007
Accepted 28 February 2008
Available online 12 April 2008

Keywords:
Ru(II)–dmso complexes
Hydrazone ligands
Trans influence
Cyclic voltammetry
Antibacterial activity
DNA-binding

ABSTRACT

The synthesis and characterization of ruthenium(II) complexes, $[RuCl_2(dmso)_2(bfmh)]$ (**1**; dmso = dimethyl sulfoxide, bfmh = benzoic acid furan-2-ylmethylene-hydrazide), $[RuCl_2(dmso)_2(btmh)]$(**2**; btmh = benzoic acid thiophen-2-ylmethylene-hydrazide), $[RuCl_2(dmso)_2(bfeh)]$(**3**; bfeh = benzoic acid (1-furan-2-yl-ethylidene)-hydrazide) and $[RuCl_2(dmso)_2(bpeh)]$(**4**; bpeh = benzoic acid (1-pyridin-2-yl-ethylidene)-hydrazide) are described. The ligands, when treated with either *cis*-$[RuCl_2(dmso)_4]$ or *trans*(Cl)–$[RuCl_2(dmso)_2(bpy)]$, resulted in the same products. This has been confirmed by IR spectra and single crystal X-ray diffraction studies. The redox behaviors of the complexes have been found to be strongly dependent on the electronic nature of the moieties present in the hydrazone ligands. The binding of the complexes to Herring sperm DNA has been studied by absorption titration and cyclic voltammetry. But, due to the random change in the absorption on the addition of DNA, only a qualitative result rather than a quantitative result has been obtained. All the complexes have been found to bind DNA through different modes to different extents. The antibacterial properties of the ligands and the complexes have been studied against five pathogenic bacteria and also the minimum inhibitory concentrations (MIC) of all the ligands and complexes **2** and **4** have been evaluated.

1. Introduction

Ruthenium complexes, launched two decades ago for antitumor therapy, are believed to have great potential as alternative drugs to cisplatin in view of their low toxicity and good selectivity for solid tumor metastasis [1]. Similar to platinum anticancer drugs, the ruthenium ion forms a covalent bond with DNA [2], affecting the replication and transcription, and leads to cell death eventually. One outstanding class of compounds which have been researched since the seventies for cancer chemotherapy is that of halogen-dimethylsulfoxide-ruthenium(II) complexes [3–6]. A well-known compound of this class, *cis*-$[RuCl_2(dmso)_4]$, has been shown to possess promising antineoplastic activity against several murine metastasizing tumors [7]. Ruthenium–dmso complexes analogous to NAMI-A (imidazolium *trans*-imidazole dimethylsulfoxide tetrachloro ruthenate) are prepared to ameliorate cisplatin activity, particularly on resistant tumors, or to reduce host toxicity at active doses [6]. Interaction with DNA, a rudimentary mechanism of action responsible for cytotoxicity, has been suggested for some ruthenium complexes [8]. At the same time, the lability of the chloro ligand in ruthenium complexes has been thought to be crucial in enhancing covalent bond formation with DNA. This paradoxical situation kindled us to synthesize new Cl–Ru–dmso complexes and to study their DNA-binding ability, followed by their anticancer activity, to arrive at a conclusion regarding their mechanism of action. To achieve this, we chose heterocyclic hydrazones as secondary ligands, since they have demonstrated potent activity against various tumor cell lines in preclinical studies, and reacted them with *cis*-$[RuCl_2(dmso)_4]$ and *trans*(Cl)–$[RuCl_2(dmso)_2(bpy)]$. The structure of the ligands is shown in Chart 1.

2. Experimental

2.1. Reagents and materials

All the chemicals used for the preparation of the ligands and buffer solution are of analytical grade or chemically pure grade. $RuCl_3 \cdot 3H_2O$, purchased from Himedia, was used as supplied. Protein free Herring sperm ds DNA, obtained from SRL chemicals, was stored at 0–4 °C and its purity was checked by measuring its optical density before use. The tris-buffer solution was prepared with

Abbreviations: ds, double stranded; TBAP, tetra butyl ammonium perchlorate; Tris, tris-(hydroxymethyl) aminomethane; UV–Vis, UV–Visible; cfu, colony forming units; NCIM, National Centre for Industrial Microorganisms; MTCC, Microbial Type Culture Collection; NCCLS, National Committee for Clinical Laboratory Standards

* Corresponding author. Tel.: +91 4222424655; fax: +91 4222422387.
E-mail address: k_natraj6@yahoo.com (K. Natarajan).

0277-5387/$ - see front matter © 2008 Elsevier Ltd. All rights reserved.
doi:10.1016/j.poly.2008.02.036

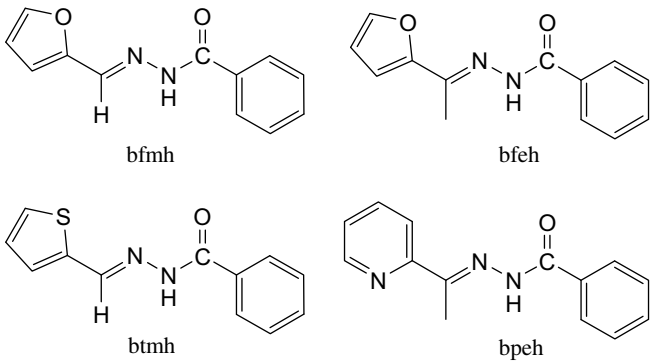

Chart 1. Structure of the hydrazone ligands.

double-distilled water and its pH was adjusted to 7.1 using 0.1 M NaOH solution. DNA stock solutions were freshly prepared before use with this buffer solution. Ethanol was purified following standard procedures for the preparation of the ligands and complexes. Distilled dmso was used for the preparation of the starting complex and for the preparation of solutions of complexes for DNA-binding studies. Purified dry methanol was used to record the electronic spectra of the complexes. Commercially available TBAP was properly dried and used as a supporting electrolyte for recording cyclic voltammograms of the complexes (except for DNA-binding studies). The starting complexes [9], *cis*-[$RuCl_2(dmso)_4$] (**Ru1**), *trans*(Cl)–[$RuCl_2(dmso)_2(bpy)$] (**Ru2**) and the ligands [10] were prepared according to the literature procedures.

2.2. Physical measurements

FT-IR spectra (4000–400 cm^{-1}) of the complexes and the free ligands were recorded as KBr pellets with a Nicolet Avatar Model FT-IR spectrophotometer. Electronic spectra (800–250 nm) of the complexes were obtained on a Systronics 119 UV–Vis spectrophotometer. ^1H NMR spectra were recorded on a Varian-Australia AMX-400. The absorption titrations were carried out with a JASCO spectrophotometer. Micro analyses (C, H, N and S) were performed on a Vario EL III Elementar analyzer. Cyclic voltammograms were recorded on a CHI 1120A electrochemical analyzer with a three electrode compartment consisting of a platinum disc working electrode, a platinum wire counter electrode and an Ag/Ag^+ reference electrode.

2.3. Synthesis

2.3.1. [$RuCl_2(dmso)_2(bfmh)$] (**1**)

Cis-[$RuCl_2(dmso)_4$] (0.21 mmol) and the ligand bfmh (0.21 mmol) were heated under reflux in ethanol for 6–8 h. Slow evaporation of the solvent after reduction to 50% gave crystals suitable for single crystal XRD studies. Yield, 70 mg, 61%. Elemental *Anal.* Calc. for $C_{16}H_{22}N_2S_2O_4Cl_2Ru$ (542.464): C, 35.42; H, 4.08; N, 5.16; S, 11.82. Found: C, 35.26; H, 4.12; N, 5.24; S, 11.37%. IR (KBr, cm^{-1}): ν(NH), 3112(w); ν(C=O), 1639(s); (νC=N), 1598(m) (s, strong; m, medium; w, weak). UV–Vis (dmso) λ, nm (ε, $mol^{-1}\,cm^{-1}\,L$): 308 (14900), 359 (3950). ^1H NMR (dmso-d_6, δ ppm): 3.2–3.5 (group of peaks, dmso protons, 12H), 8.1 (s, H–C=N, 1H), 7.5–8.1 (multiplet, aromatic protons, 8H), 9.2 (s, –NH, 1H).

2.3.2. [$RuCl_2(dmso)_2(bfmh)] \cdot 0.5C_2H_5OH$ (**1a**)

trans(Cl)–[$RuCl_2(dmso)_2(bpy)$] (0.21 mmol) and the ligand bfmh (0.21 mmol) were heated under reflux in ethanol for 6–8 h. Slow evaporation of the solvent after reduction to 50% gave crystals suitable for single crystal XRD studies. Yield, 69 mg, 58%. Elemental *Anal.* Calc. for $C_{17}H_{25}N_2S_2O_{4.5}Cl_2Ru$ (565.494): C, 36.10; H, 4.45; N, 4.95; S, 11.34. Found: C, 35.92; H, 4.33; N, 4.71; S, 11.27%. IR (KBr, cm^{-1}): ν(NH), 3110(w); ν(C=O), 1639(s); (νC=N), 1598(m).

2.3.3. [$RuCl_2(dmso)_2(btmh)$] (**2**)

Cis-[$RuCl_2(dmso)_4$] (0.21 mmol) and the ligand btmh (0.21 mmol) were heated under reflux in ethanol for 6–8 h. Slow evaporation of the solvent after reduction to 50% gave orange crystals suitable for single crystal XRD studies. Yield, 75 mg, 64%. Elemental *Anal.* Calc. for $C_{16}H_{22}N_2S_3O_3Cl_2Ru$ (558.531): C, 34.40; H, 3.97; N, 5.01; S, 17.22. Found: C, 34.28; H, 3.87; N, 5.32; S, 17.37%. IR (KBr, cm^{-1}): ν(NH), 3080(w); ν(C=O), 1620(s); ν(C=N), 1592(m). UV–Vis (dmso) λ, nm (ε, $mol^{-1}\,cm^{-1}\,L$): 254 (25320), 313 (19320), 392 (5480). ^1H NMR (dmso-d_6, δ ppm): 3.2–3.5 (group of peaks, dmso, 12H), 7.9 (s, H–C=N, 1H), 7.4–8.5 (multiplet, aromatic protons, 8H), 9.4 (s, –NH, 1H). The same reaction when carried out with *trans*(Cl)–[$RuCl_2(dmso)_2(bpy)$] yielded a crystalline product (**2a**) which conformed to the analytical and IR data of **2** but was not structurally characterized.

2.3.4. [$RuCl_2(dmso)_2(bfeh)$] (**3**)

Cis-[$RuCl_2(dmso)_4$] (0.21 mmol) and the ligand bfeh (0.21 mmol) were heated under reflux in ethanol for 6–8 h. Slow evaporation of the solvent gave only an amorphous powder which was recrystallised from hot dmso. Yield, 69 mg, 59%. Elemental *Anal.* Calc. for $C_{17}H_{24}N_2S_2O_4Cl_2Ru$ (556.491): C, 36.69; H, 4.34; N, 5.03; S, 11.52. Found: C, 36.28; H, 4.02; N, 5.39; S, 11.11%. IR (KBr, cm^{-1}): ν(NH), 3073(w); ν(C=O), 1650(s); ν(C=N), 1593(m). UV–Vis (dmso) λ, nm (ε, $mol^{-1}\,cm^{-1}\,L$): 288 (9780), 354 (2620). ^1H NMR (dmso-d_6, δ ppm): 3.1–3.4 (group of peaks, dmso, 12H), 2.2 (s, $-CH_3$, 3H), 7.2–8.2 (multiplet, aromatic protons, 8H), 9.4 (s, –NH, 1H). The same reaction when carried out with *trans*(Cl)–[$RuCl_2(dmso)_2(bpy)$] yielded an amorphous product (**3a**) which conformed to the analytical and IR data of **3**.

2.3.5. [$RuCl_2(dmso)_2(bpeh)$] (**4**)

Cis-[$RuCl_2(dmso)_4$] (0.21 mmol) and the ligand bpeh (0.21 mmol) were heated under reflux in ethanol for 6–8 h. Slow evaporation of the solvent gave only an amorphous powder which was recrystallised from hot dmso. Yield, 82 mg, 69%. Elemental *Anal.* Calc. for $C_{18}H_{25}N_3S_2O_3Cl_2Ru$ (567.518): C, 38.09; H, 4.40; N, 7.40; S, 11.30. Found: C, 38.44; H, 4.32; N, 7.12; S, 11.47%. IR (KBr, cm^{-1}): ν(NH), 3056(w); ν(C=O), 1689(s); ν(C=N), 1598(m). UV–Vis (dmso) λ, nm (ε, $mol^{-1}\,cm^{-1}\,L$): 275 (7540), 304 (5700). ^1H NMR (dmso-d_6, δ ppm): 3.1–3.4 (group of peaks, dmso, 12H), 2.2 (s, $-CH_3$, 3H), 7.3–8.3 (multiplet, aromatic protons, 9H), 9.4 (s, –NH, 1H). The same reaction when carried out with *trans*(Cl)–[$RuCl_2(dmso)_2(bpy)$] yielded an amorphous product (**4a**) which conformed to the analytical and IR data of **4**.

2.4. Crystallographic structure determination

Single crystal X-ray diffraction measurements were performed on a Nonius Kappa CCD (with Oxford Cryostream) diffractometer with graphite monochromatized Mo Kα radiation. The structures of **1** and **2** were solved by direct methods and refinements were carried out by full-matrix least-square techniques. The hydrogen atoms were treated by a mixture of independent and constrained refinement. The following computer programs were used: structure solution SIR-97 [11], refinement SHELXL-97 [12], molecular diagrams ORTEP-3 [13] for windows.

2.5. Anti-microbial screening

The bacterial strains, *Escherichia coli* NCIM 2831, *Staphylococcus aureus* NCIM 2492, *Staphylococcus epidermidis* NCIM 2493,

Klebsiella pneumoniae NCIM 5082 and *Shigella sonnei* MTCC 2957 were used in the study. The agar-well diffusion method [14] was employed for the determination of anti-microbial activities. MICs (minimum inhibitory concentration) of the compounds against test organisms were determined by the broth micro dilution method. All the tests were performed in duplicate and repeated twice. Modal values were selected.

2.5.1. Agar-well diffusion method

The compounds were weighed and dissolved in dimethyl sulfoxide (dmso), then the solutions were filter sterilized using a 0.45 μm membrane filter. Each microorganism was suspended in sterile saline and diluted at *ca.* 106 colony forming units (cfu/ml). They were flood inoculated onto the surface of Mueller–Hinton Agar (MHA). The wells (8 mm in diameter) were cut from the agar and 0.1 mL of solution was delivered into them. After incubation for 24 h at 37 °C, all the plates were examined for any zones of growth inhibition, and the diameter of these zones were measured in millimeters.

2.5.2. Determination of minimum inhibitory concentration (MIC)

A broth microdilution susceptibility assay was used as recommended [15] by NCCLS for determination of the MIC. All the tests were performed in Mueller–Hinton Broth (MHB) supplemented with Tween 80 detergent (final concentration 0.5% (v/v)). Bacterial strains were cultured overnight at 37 °C in MHA. Test strains were suspended in MHB to give a final density of 5×105 cfu/ml and these were confirmed by viable counts. Geometric dilutions of the compounds were prepared in a 96-well microtiter plate, including one growth control (MHB + Tween 80) and one sterility control (MHB + Tween 80 + compound). The plates were incubated under normal atmospheric conditions at 37 °C for 24 h. The MIC of kanamycin and oxytetracycline were individually determined in parallel experiments in order to control the sensitivity of the test organisms. The bacterial growth was indicated by the presence of a white "pellet" on the well bottom.

3. Results and discussion

The reactions of either **Ru1** or **Ru2** with the hydrazone ligands in a 1:1 mol ratio in ethanol has yielded complexes of the type $[RuCl_2(dmso)_2(L)]$ (L = hydrazone ligand), as illustrated in Scheme 1. All the complexes are stable to air and light, and are soluble in organic solvents such as dmso, dmf and dichloromethane. The hydrazone ligands act as neutral bidentate donors replacing two dmso ligands from **Ru1**. In the precursor **Ru2**, there is a bipyridine chelate and two S-bonded dmso ligands in the equatorial plane. Although the chelate effect should hinder the replacement of the bpy ligand from **Ru2**, the two mutually *cis* S-bonded dmso ligands that are capable of accepting π-back donated electrons from the metal, along with the larger trans influence, weakens the metal-N bonds, facilitating the replacement of the chelate [16].

3.1. IR and electronic spectra

The IR spectra of the free ligands and the new Ru(II) complexes were compared in order to ascertain the probable mode of coordination of the ligands. Vibration bands of primary importance of the free ligands were observed around 3250, 1650, 1600–1620 and 1080 cm^{-1} for ν(NH), ν(CO), ν(CN) and ν(NN) respectively. The presence of the ν(NH) band confirms that the free ligands are in the keto form. The IR spectra of the complex pairs **1** and **1a**, **2** and **2a**, **3** and **3a**, and **4** and **4a** were identical, suggesting the formation of the same complexes when the ligands are treated with either **Ru1** or **Ru2**. None of the complexes obtained from **Ru2** displayed a pyridine ring breathing band around 995 cm^{-1}, which implies the replacement of bpy from **Ru2** by the ligands. This directed us to formulate the complexes in general as $[RuCl_2(dmso)_2(L)]$(L = bfmh, bfeh, btmh or bpeh). In all of the complexes, the observed significant decrement of ν(CO) and ν(CN) does evidence the neutral bidentate nature of the ligands. Being so, the ligands have two possibilities for chelation with the metal, either replacing two S-bonded dmso ligands or one S-bonded and one O-bonded dmso ligand when treated with **Ru1**. Scrutinizing the IR spectra of the precursor *cis*-$[RuCl_2(dmso)_4]$ and that of the new complexes was useful in determining the elimination of one of the above possibilities. In the IR spectrum of *cis*-$[RuCl_2(dmso)_4]$, the S=O stretch of the S-bonded dmso appears at a higher frequency (1090 cm^{-1}) in comparison with that of the O-bonded dmso (915 cm^{-1}) due to the increase in the S=O bond order in the former case. The desertion and retention of the bands at 915 cm^{-1} and around 1090 cm^{-1} respectively in the new complexes indicate the replacement of one O-bonded and one S-bonded dmso ligand from the precursor by the Schiff base chelate. This is consistent with the previous observation that chelating ligands will replace first the weakly held O-bonded dmso and then the S-bonded dmso *cis* to it [9].

The absorption spectra of the diamagnetic Ru(II) complexes were recorded as 10^{-4} M dmso solutions in the range 800–250 nm using a quartz cuvette of 1 cm path length. All the new ruthenium(II) complexes, except **4**, exhibit bands in both UV and visible regions. Based on the position and nature of the peaks, all the bands are assigned to either $n \rightarrow \pi^*$ or $\pi \rightarrow \pi^*$ intraligand transitions (data given in experimental section).

3.2. X-ray crystallography

Though slow evaporation of the respective reaction mixtures yielded X-ray quality single crystals of **1**, **1a**, **2** and **2a**, only structures of the first three complexes were solved. Structure determination of **1** and **1a** showed that the two compounds are one and the same, as the unit cell parameters of the two complexes were very close and other structural features and geometric parameters were similar. The crystal data and data collection procedure are supplied in Table 1. Selected geometrical parameters are listed in Table 2. Figs. 1 and 2 show the ORTEP diagrams of **1** and **2** respectively. In both of the complexes, there are two independent

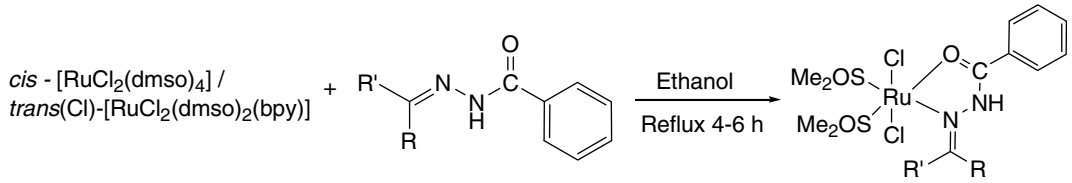

Scheme 1. Synthesis of the new Cl–Ru(II)–dmso complexes

Table 1
Crystal structure data of the complexes **1** and **2**

Crystal data	**1**	**2**
Formula	$C_{16}H_{22}Cl_2N_2O_4RuS_2 \cdot 0.5(C_2H_6O)$	$C_{16}H_{22}Cl_2N_2O_3RuS_3 \cdot 0.5(C_2H_6O)$
Formula weight	565.48	581.54
Color, habit	colorless, fragment	orange, parallelepiped
Dimensions	0.23 × 0.20 × 0.12 mm	0.25 × 0.10 × 0.05 mm
Space group	$P\bar{1}$	$P\bar{1}$
a (Å)	11.2248(11)	11.0411(15)
b (Å)	14.1644(15)	14.2763(16)
c (Å)	14.663(2)	15.1254(16)
α (°)	92.762(4)	92.617(7)
β (°)	98.201(3)	100.003(7)
γ (°)	103.233(8)	104.928(5)
V (Å^3)	2238.3(4)	2258.4(5)
Z	4	4
D_{calc} (Mg m^{-3})	1.678	1.710
T (K)	110	115
F_{000}	1148	1180
μ(Mo Kα) (mm^{-1})	1.154	1.232
R_{int}	0.075	0.035
Goodness of fit (S)	1.077	1.024
θ_{max} (°)	32.5	30.6

complexes (**A** and **B**) in the asymmetric units and a disordered solvent molecule. Refinement of the disordered regions of both **1** and **2** has been carried out, but the fit to the data did not really improved in either case, nor were there any significant changes in the interesting parts of the structure.

In complex **1**, the ruthenium(II) ion is in a distorted octahedral environment equatorially coordinated by an ON chelate of the hydrazone ligand and two sulfur atoms of the dmso ligands at *cis* positions. A pair of chlorine atoms at the axial positions completes the octahedral coordination. The Ru–N (Ru1a–N1a = 2.107(2) and Ru1b–N1b = 2.098(3) Å) and Ru–O (Ru1a–O1a = 2.123(2) and Ru1b–O1b = 2.101(2) Å) bond lengths observed in the two independent complexes are comparable to literature values [17–23]. The two Ru–S bond lengths observed in the independent complexes **A** and **B** are comparable with that of similar Ru(II) complexes [17] and with that of the precursor, *cis*-[$RuCl_2(dmso)_4$] [24]. As expected and previously observed [24,25] there is a change in the S–O bond length of dmso after coordination in comparison with the free ligand.

The substitution of one O-bonded dmso and one S-bonded dmso in the precursor *cis*-[$RuCl_2(dmso)_4$] by the ON chelating ligand has yielded **1** in which the two chloro ligands take mutual *trans* positions, which is in accordance with a previous study [17]. The two Cl ligands in the axial positions are faintly bent to-

Table 2
Selected geometrical parameters for **1** and **2**

Bond distances (Å)			Bond angles (°)		
	1	**2**		**1**	**2**
Ru1a–N1a	2.107(2)	2.107(2)	Cl1a–Ru1a–Cl2a	174.30(3)	173.95(3)
Ru1a–O1a	2.123(2)	2.115(2)	S1a–Ru1a–S2a	94.50(3)	94.69(3)
Ru1a–S1a	2.2242(9)	2.2304(8)	N1a–Ru1a–O1a	77.31(9)	77.12(8)
Ru1a–S2a	2.2584(8)	2.2487(7)	Cl1b–Ru1b–Cl2b	172.28(3)	172.06(3)
Ru1a–Cl1a	2.4174(8)	2.4054(8)	S1b–Ru1b–S2b	94.14(3)	94.52(3)
Ru1a–Cl2a	2.3959(8)	2.3964(8)	N1b–Ru1b–O1b	77.86(9)	77.54(9)
Ru1b–N1b	2.098(3)	2.083(2)	C13a–S1a–C14a	100.09(16)	99.55(16)
Ru1b–O1b	2.101(2)	2.088(2)	C15a–S2a–C16a	99.1(2)	98.67(18)
Ru1b–S1b	2.2297(9)	2.2264(8)	C13b–S1b–C14b	99.17(17)	99.54(15)
Ru1b–S2b	2.2453(9)	2.2547(8)	C15b–S2b–C16b	98.7(2)	99.71(17)
Ru1b–Cl1b	2.3934(8)	2.4037(7)	C13a–S1a–O3a	104.07(15)	104.78(16)
Ru1b–Cl2b	2.4091(8)	2.4095(8)	C14a–S1a–O3a	106.34(16)	106.63(16)
S1a–O3a	1.489(2)	1.485(2)	C15a–S2a–O4a	106.28(16)	106.03(15)
S2a–O4a	1.486(2)	1.490(2)	C16a–S2a–O4a	106.75(17)	106.43(16)
S1b–O3b	1.493(3)	1.497(2)	C13b–S1b–O3b	107.37(17)	106.71(14)
S2b–O4b	1.487(3)	1.490(2)	C14b–S1b–O3b	105.56(17)	104.90(14)
			C15b–S2b–O4b	107.18(17)	106.73(16)
			C16b–S2b–O4b	106.3(2)	104.91(13)

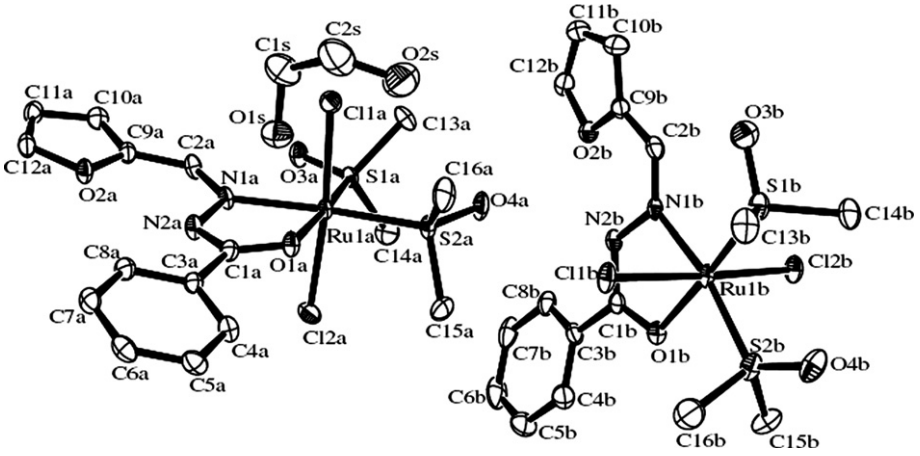

Fig. 1. Asymmetric unit of **1** with anisotropic displacement ellipsoids at 50% probability. Hydrogen atoms are omitted for clarity.

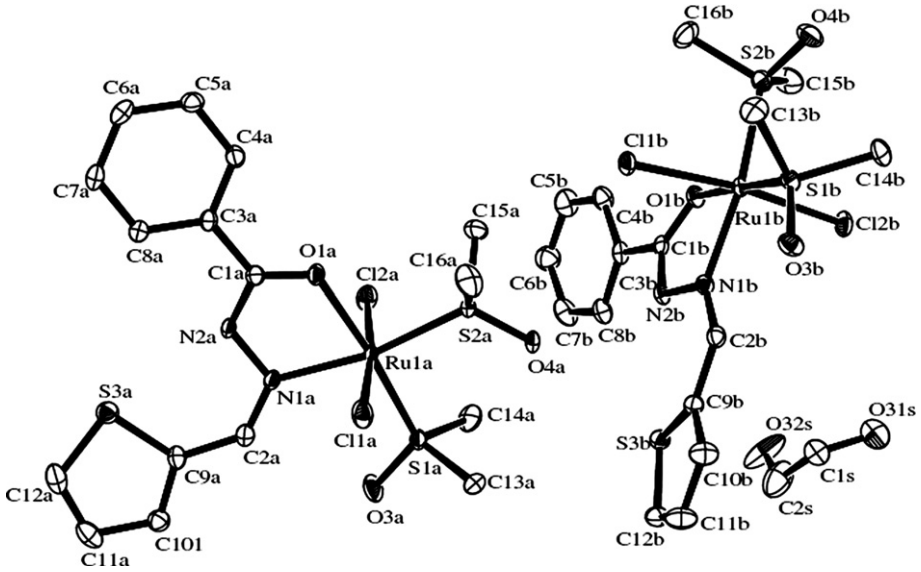

Fig. 2. Asymmetric unit of **2** with anisotropic displacement ellipsoids at 50% probability. Hydrogen atoms and disorder in thiophene ring are omitted for clarity.

wards the chelate (the angle Cl2a–Ru1a–Cl1a is 174.30(3)° and Cl2b–Ru1b–Cl1b is 172.28(3)°) due to the pushing by the somewhat bulky *cis* dmso ligands. The Ru–Cl distances in **1** (Ru1a–Cl1a = 2.4174(8), Ru1a–Cl2a = 2.3959(8) Å; Ru1b–Cl1b = 2.3934(8), Ru1b–Cl2b = 2.4091(8) Å) are shorter than that of **Ru1** (mean Ru–Cl distance of the different forms is 2.425 Å) and fairly comparable with that of **Ru2** (2.402 Å). This is in agreement with the greater trans influence of dmso [24].

The angles O–S–C and C–S–C in **A** and **B** of **1** are comparable with that of the S-bonded dmso ligands in *cis*- and *trans*-$[RuCl_2(dmso)_4]$. But these angles of O-bonded dmso in one of the precursors, **Ru1**, is relatively narrow when compared with that of S-bonded dmso ligands. This is due to the different electronic situation of the two types of sulfur atom and can be attributed to the compression effect of the bulkier lone pair of the pyramidal sulfur atoms on the bonding pairs [25]. The bite angles of the ON chelate in **A** and **B** are 77.31(9) and 77.86(9)° respectively, and these are comparable with that of a similar chelate [17].

The structure of **2** shares similar properties and the same discussion goes well with that for **1** except in a few aspects. The heterocyclic ring in **1** is furan whereas in **2** it is thiophene and there is a slight distortion in the thiophene moiety in one of the two independent complexes. Further refinement, using a number of restraints, of the disordered thiophene led to a slight improvement, most notably in the reduction of residual electron densities. However, full anisotropic refinement did not lead to realistic displacement parameters. The independent complexes in the asymmetric units of **1** are stabilized by intramolecular N(amide)–H···O(furan) bonds and intermolecular N(amide)–H···O(dmso) bonds in addition to bifurcated weak interactions, O(disordered ethanol)–H···Cl and O(disordered ethanol)–H···O(furan). In contrast to **1**, intermolecular hydrogen-bonding, N(amide)–H···O(dmso) appears to be predominant in complex **2**. The geometric parameters pertaining to hydrogen-bonding are provided in Table 3.

With the single crystal X-ray structures of **1** and **1a**, it is clear that the chelating ligands replace the coordinated ligands that are *trans* to the two S-bonded dmso from either of the precursors **Ru1** and **Ru2**. This is due to the strong *trans* influence of the S-bonded dmso ligands. Also, in **Ru2**, the chelating bpy ligands are replaced by the ON hydrazone chelate relatively easily compared to the two S-bonded dmso ligands because of the strong π-acceptor character of the two sulfur atoms. Hence, the complex pairs **2** and **2a**, **3** and **3a**, and **4** and **4a** will be mentioned henceforth as **2**, **3** and **4** respectively assuming that they have same chemical composition (based on the microanalyses) although no structural evidence is currently available for the other complexes.

Table 3
Hydrogen-bonding distances (Å) and angles (°)

Complex	D–H···A	D–H	H···A	D···A	D–H···A
1	N2a–H2Na···O2a	0.77(4)	2.28(4)	2.750(3)	120(3)
	N2b–H2Nb···O4a	0.87(4)	2.14(4)	2.917(3)	149(3)
	N2b–H2Nb···O2b	0.87(4)	2.21(4)	2.682(3)	114(3)
2	N2a–H2Na···O3b[i]	0.85(4)	2.18(4)	2.988(3)	159(3)
	N2b–H2Nb···O4a	0.85(3)	1.96(3)	2.803(3)	167(3)

[i] Symmetry codes used to generate identical atoms: x, y − 1, z.

3.3. ^1H NMR spectra

The ^1H NMR spectra of the complexes recorded in dmso showed narrow signals typical for diamagnetic Ru(II) complexes. A comparison of the ^1H NMR data [9] of the precursor *cis*-$[RuCl_2(dmso)_4]$ with that of the new complexes seems indispensable in order to ascertain the bonding mode of the two dmso ligands, as evidenced by the single crystal X-ray diffraction studies (for **1** and **2**), and to predict the same in **3** and **4**. The resonance for methyl protons of free dmso is ~δ 2.5 ppm. The complex *cis*-$[RuCl_2(dmso)_4]$ (contains three S-bonded dmso and one O-bonded dmso) displayed six singlets at δ 3.50, 3.48, 3.43, 3.32, 2.72 and 2.66 ppm due to six sets of chemically different protons. The peak at δ 2.66 ppm has been assigned to free dmso which resulted from the 10% dissociation of O-bonded dmso. Similarly the peak at δ 2.72 ppm has been attributed to the O-bonded dmso since the methyl resonance is close to that of free dmso. The other peaks appearing in a group have been assigned to S-bonded dmso but the integration of these peaks had not been possible owing to their proximity and their sharing of the same broad base line. The three S-bonded dmso ligands in the complex are *trans* to either O-bonded dmso, S-bonded dmso or Cl ligands. This, along with some degree of methyl inequivalency, has been thought of as responsible for the complexity of the spectra. Keeping all these in mind, the group of peaks appearing in the new complexes around ~δ 3.2–3.4 ppm is attributed to S-bonded dmso resonances. Here no resonance was observed at δ

2.7 ppm for any of the complexes, suggesting that there is no O-bonded dmso in the complexes which is consistent with the single crystal X-ray diffraction results obtained for **1** and **2**, and predicts the same for **3** and **4**. Thus the inequivalency in the methyl groups is due to the chelating ligand. The resonance around δ 2.5 ppm in all the complexes is due to the solvent. The azomethine proton in **1** and **2** appears as a singlet at δ 8.1 and 7.9 ppm respectively. The protons of the methyl group in **3** and **4** gave a resonance at δ 2.2 ppm. The multiplet around δ 7.2–8.5 ppm is due to aromatic and heterocyclic ring protons. The appearance of a singlet in all the complexes around δ 9.2–9.4 ppm is due to the NH proton and this suggests that the chelating ligand coordinates in its keto form to the metal and supports a neutral bidentate coordination of the hydrazone ligands.

3.4. Cyclic voltammetric studies

The electrochemical behavior of the complexes was studied with the help of cyclic voltammetry using dmso solutions of the complexes and TBAP as a supporting electrolyte. All the potentials were referenced to the Ag/AgCl electrode and scanned at a rate of 0.1 V/s. The complexes show different redox behavior in the chosen potential window. Complexes **1** and **4** show only a Ru^{III}/Ru^{II} oxidation couple with the formal potentials 0.63 and 0.50 V respectively. Complex **2** shows only an irreversible oxidation wave with E_{pa} = 0.49 V. This irreversibility may be anticipated due to the transient lifetime of the reduced state. The peak-to-peak separation value ΔE_p for **1** and **4** is 240 and 80 mV suggesting a quasireversible and reversible one electron transfer process respectively. A reversible reduction (Ru^{II}/Ru^{I}) is observed for **3** with a formal potential of −0.39 V (ΔE_p = 80 mV). These different conducts of the complexes can be accredited to the different electronic nature of the substituents present in the hydrazone ligands. When the E_f values for the oxidation couple for **1** and **4** are compared, a negative shift in the potential is observed. This shift is due to the presence of an electron releasing CH_3 group and pyridine moiety in **4** which favor easier oxidation of the central metal ion. The more electron withdrawing furan ring of **3** renders the molecule prone to reduction of the ruthenium centre [26]. In summary it can be drawn that electron releasing substituents stabilize the +3 oxidation state whereas electron withdrawing substituents stabilize the +2 oxidation state of ruthenium.

3.5. DNA-binding studies

Most ruthenium complexes bind to DNA by non-covalent interactions such as electrostatic binding, groove binding, intercalative binding and partial intercalative binding [27]. A quantitative understanding of the factors that determine the recognition of DNA sites would be valuable in the rational drug design of new DNA targeted molecules for application in chemotherapy. The binding of the new ruthenium complexes to the Herring sperm ds DNA has been monitored through absorption titration and cyclic voltammetry.

3.5.1. Absorption titration

The experiments were carried out in Tris–HCl buffer (50 mM,pH 7.2) using a solution of Herring sperm DNA which gave a ratio of UV absorbance at 260 and 280 nm in the ratio 1.8:1, indicating that the DNA is sufficiently free from protein. So no further effort was made to purify the commercially obtained DNA. The concentration of DNA was determined by absorption spectroscopy using the ε value of 6600 M^{-1} cm^{-1} at 260 nm. Absorption titrations were performed using a fixed ruthenium concentration to which increments of the DNA stock solutions were added in different ratios ranging from 0 to 3 [DNA]/[Ru]. Complex–DNA solutions were allowed to stand for 5 min before recording their absorption. The titration process was repeated until no further change was observed in the spectra.

The binding of the ruthenium complexes to the DNA helix was characterized by following the changes in the absorbance and shift in wavelength upon each addition of DNA solution to the complex. Representative absorption spectra are given in Figs. 3 and 4. The ruthenium(II) complexes in dmso-buffer mixture exhibit an intense intraligand transition in the region around 315–330 nm. On the titration of Herring sperm DNA with the complexes, a considerable increase or decrease in the absorption along with a small red or blue shift was observed. The initial increase in absorption for complexes **2** and **3** is due to the electrostatic interaction of DNA and the complexes [28]. In complexes **2** and **4** remarkable hypochromicity is noted after the ratio [DNA]:[Ru] becomes 1. In complex **1** the absorption decreases and increases at random with a small red shift (2–4 nm) on titration with the DNA solution. These trends show that the complexes bind to the DNA double-helix in different modes to different extents [29]. As can be perceived from Figs. 3 and 4, the shift in absorption and λ_{max} are random and this tendency frustrated the calculation of intrinsic binding constants of the complexes using the equation valid for perfect intercalators.

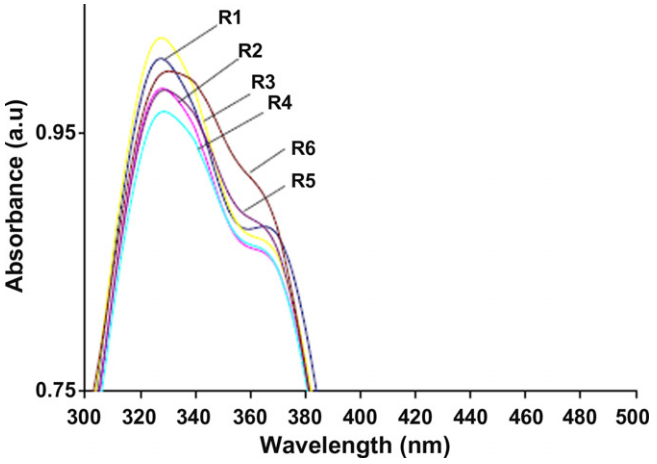

Fig. 3. Absorption bands of **1** on titration with DNA at different [DNA]/[Ru] ratios (*R*). *R*1 = 0, *R*2 = 0.25, *R*3 = 0.50, *R*4 = 0.75, *R*5 = 1 and *R*6 = 1.5.

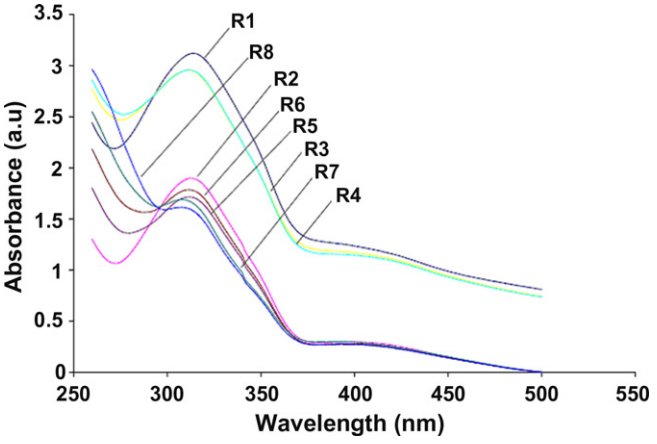

Fig. 4. Absorption bands of **4** on titration with DNA at different [DNA]/[Ru] ratios (*R*). *R*1 = 0, *R*2 = 0.25, *R*3 = 0.50, *R*4 = 0.75, *R*5 = 1, *R*6 = 1.5, *R*7 = 2 and *R*8 = 3.

Table 4
Antibacterial activity data for the ligands and complexes

Compound	*Escherichia coli*		*Shigella sonnei*		*Staphylococcus aureus*		*Staphylococcus epidermidis*		*Klebsiella pneumoniae*	
	WD[a]	MIC[b]	WD	MIC	WD	MIC	WD	MIC	WD	MIC
2	NA	136	17	74	12	31	14	46	NA	144
4	NA	121	NA	82	16	153	15	32	NA	140
bfmh	15	25	20	28	16	18	12	26	15	47
btmh	NA	85	16	97	NA	44	14	87	NA	124
bfeh	30	24	33	26	26	21	20	23	30	28
bpeh	20	23	25	34	NA	137	14	92	20	52
Oxytetracycline	30	15	37	8	32	7	44	8	30	8
Kanamycin	32	18	48	9	40	10	60	11	35	10

NA – not active.
[a] WD, disc diffusion method as recommended by NCCLS. Diameter of zone of inhibition (mm) including well diameter 8 mm. 100 μg of both compound and antibiotics were used.
[b] MIC, minimum inhibitory concentration.Values given as μg/ml for both compounds and antibiotics.

3.5.2. Cyclic voltammetry

Since all the new complexes are electroactive, electrochemical methods such as cyclic voltammetry can be used effectively to monitor their binding to DNA as a complement to the absorption spectral technique. In a typical cyclic voltammetric titration, a fixed concentration of the complex was taken and DNA solution in buffer was added in different ratios as done in the absorption titration, and the voltammetric response was recorded. As observed in the UV experiments, an increase or decrease of the peak current was observed for all the complexes. The peak current increased initially and then decreased. The initial increase in the peak current is due to the absorption of the DNA bound complex onto the electrode surface [30]. The decrease in peak current on the addition of DNA to the complex is suggestive of an interaction between the complex and DNA [31]. Except for complex **1**, a decrease in the peak-to-peak separation was observed, which is consistent with non-coordinating intercalative binding of the complexes through the planar aromatic rings between the DNA base pairs [32]. The formal potential E_f shifts slightly towards the positive side and is attributed to characteristic behavior of intercalation of the complexes into the DNA double-helix [33], and suggests that Ru(II) and Ru(I) forms bind to DNA at different rates [34,35].

3.6. Antibacterial activity

All the ligands and their ruthenium complexes were screened *in vitro* for their growth inhibitory activity against the pathogenic bacteria *E. coli*, *S. aureus*, *S. epidermidis*, *K. pneumoniae* and *S. sonnei*. The inhibition zone (in mm) and MIC of the ligands and their ruthenium complexes are given in Table 4. From the figures it is perceived that the ligands bfmh and btmh inhibit the growth of all the test organisms to a moderately comparable extent to that of standard antibiotics and they can be said to be resistive to the organisms. The ligand btmh is resistive only to *S. sonnei* and *S. epidermidis* since no inhibition zone is found for the other organisms. Except for *S. aureus*, the ligand bpeh is resistive to all other pathogenic bacteria. All the complexes except **3** are resistive to at least one of the organisms under study. Complex **2** shows considerable resistivity to *S. aureus*, *S. epidermidis* and *S. sonnei*. Similarly **4** is active against *S. aureus* and *S. epidermidis* and **1** is active against only *S. sonnei*. None of the complexes are active against the other two organisms. Thus all the ligands and complexes **2** and **4** alone have been studied further to evaluate the MIC because only these two complexes demonstrate activity against at least two of the five organisms. A low value of MIC implies high resistivity against the particular organism. No serious attempts were made to correlate the activity to the structures of the compounds since too many chemical and biochemical factors are responsible for the process of inhibition of the growth of the bacteria.

4. Conclusions

The present study demonstrates a simplistic synthesis of a family of new Cl–dmso–Ru(II) complexes. The greater *trans* influence of mutually *cis* S-bonded dmso ligands in comparison to the bipyridine ligand has been proved by the observed replacement of bipyridine from **Ru2** by the hydrazone ligands, with crystallographic evidence. The electrochemical properties of the complexes are very sensitive to the electronic nature of the substituents present in the hydrazone ligands. The new complexes have been shown to possess DNA-binding abilities. The *in vitro* antineoplastic activity of the complexes against human breast cancer cell lines is under investigation and the results will be published shortly.

Appendix A. Supplementary data

CCDC 613460 and 632085 contain the supplementary crystallographic data for **1** and **2**. These data can be obtained free of charge via http://www.ccdc.cam.ac.uk/conts/retrieving.html, or from the Cambridge Crystallographic Data Centre, 12 Union Road, Cambridge CB2 1EZ, UK; fax: (+44) 1223-336-033; or e-mail: deposit@ccdc.cam.ac.uk. Supplementary data associated with this article can be found, in the online version, at doi:10.1016/j.poly.2008.02.036.

References

[1] G. Sava, S. Pacer, A. Bergamo, M. Cocchettio, G. Mestroni, E. Alessio, Chem.-Biol. Interact. 95 (1995) 109.
[2] E. Wong, C.M. Giandomenico, Chem. Rev. 99 (1999) 2451.
[3] D.P. Riley, Inorg. Chem. 22 (1983) 1965.
[4] D.P. Riley, R. Shumate, J. Am. Chem. Soc. 106 (1984) 3179.
[5] D.P. Riley, J.D. Oliver, Inorg. Chem. 25 (1986) 1814.
[6] A. Bergamo, G. Stocco, C. Casarsa, M. Cocchettio, E. Alessio, B. Serli, S. Zorzet, G. Sava, Int. J. Oncol. 24 (2004) 373.
[7] G. Sava, S. Zorzet, T. Giraldi, G. Mestroni, G. Zessinovich, Eur. J. Cancer Clin. Oncol. 20 (1984) 841.
[8] S. Zorzet, A. Bergamo, M. Cocchettio, A. Sore, B. Gava, E. Alessio, E. Iengo, G. Sava, J. Pharmacol. Expl. Ther. 295 (2000) 927.
[9] I.P. Evans, A. Spencer, G. Wilkinson, J. Chem. Soc., Dalton Trans. (1973) 204.
[10] M.F. Iskander, L. Labib, M.M.Z. Nour El-Din, M. Tawfik, Polyhedron 8 (1989) 2755.
[11] A. Altomare, M.C. Burla, M. Camalli, G. Cascarano, C. Giacovazzo, A. Guagliardi, A.G.G. Moliterni, G. Polidori, R. Spagna, J. Appl. Crystallogr. 32 (1999) 115.
[12] G.M. Sheldrick, SHELXL-97. A Program for Structure Refinement, University of Göttingen, Göttingen, Germany, 1997.

[13] L.J. Farrugia, J. Appl. Crystallogr. 30 (1997) 565.
[14] NCCLS (National Committee for Clinical Laboratory Standards), Performance standards for antimicrobial disk susceptibility test, 6th ed., Approved standard, Wayne Pa., M2-A6, 1997.
[15] NCCLS (National Committee for Clinical Laboratory Standards), Performance standards for antimicrobial susceptibility testing, Ninth International Supplement, Wayne Pa. M100-S9, 1999.
[16] M. Ghassemzadeh, M. Bolourtchian, S. Chitsaz, B. Neumüller, M.M. Heravi, Eur. J. Inorg. Chem. 8 (2000) 1877.
[17] L. Otero, P. Nobilia, D. Gambino, H. Cerecetto, M. González, J.A. Ellena, O.E. Piro, Inorg. Chim. Acta 344 (2003) 85.
[18] R. Cini, G. Tamasi, S. Defazio, M. Corsini, P. Zanello, L. Messori, G. Marcon, F. Piccioli, R. Orioli, Inorg. Chem. 42 (2003) 8038.
[19] Q.A. de Paula, A.A. Batista, O.R. Nascimento, A.J. da Costa-Filho, M.S. Schultz, M.R. Bonfadini, G. Oliva, J. Braz. Chem. Soc. 11 (5) (2000) 530.
[20] R.E. Morris, R.E. Arid, P.D.S. Murdoch, H. Chen, J. Cummings, N.D. Hughes, S. Parson, A. Parkin, G. Boyd, D.I. Jodrell, P.J. Sadler, J. Med. Chem. 44 (2001) 3616.
[21] P. Braunstein, C. Graiff, F. Naud, A. Pfaltz, T. Tiripicchio, Inorg. Chem. 39 (2000) 4468.
[22] S.A. Serron, C.M. Haar, S.P. Nolan, Organometallics 16 (1997) 5120.
[23] R.C. van der Drift, E. Bouwman, E. Drent, H. Kooijman, A.L. Spek, A.B. van Oort, W.P. Mul, Organometallics 21 (2002) 3401.
[24] E. Alessio, G. Mestroni, G. Nardin, W.M. Attia, M. Calligaris, G. Sava, S. Zorzet, Inorg. Chem. 27 (1998) 4099.
[25] E. Alessio, G. Balducci, M. Calligaris, G. Costa, W.M. Attia, G. Mestroni, Inorg. Chem. 30 (1991) 609.
[26] A.R. Cowley, J.R. Dilworth, P.S. Donnelly, J.M. White, Inorg. Chem. 45 (2006) 496.
[27] J.K. Barton, Science 233 (1986) 727.
[28] P.R. Reddy, V. Radhika, K.S.J. Rao, Chem. Sci. 116 (4) (2004) 221.
[29] S. Ramakrishnan, M. Palaniandavar, J. Chem. Sci. 117 (2) (2005) 179.
[30] X.M. Li, H.Q. Ju, C.F. Ding, S.S. Zhang, Anal. Chim. Acta 582 (1) (2007) 158.
[31] Z.S. Yang, Y.L. Wang, G.C. Zhao, Anal. Sci. 20 (2004) 1127.
[32] J. Annaraj, S. Srinivasan, K.M. Ponvel, K.P.R. Athappan, J. Inorg. Biochem. 99 (2005) 669.
[33] X. Lu, M. Zhang, J. Kang, X. Wang, L. Zhuo, H. Liu, J. Inorg. Biochem. 98 (2004) 582.
[34] S. Srinivasan, J. Annaraj, P.R. Athappan, J. Inorg. Biochem. 99 (2005) 876.
[35] V.G. Vaidyanathan, B.U. Nair, J. Chem Soc., Dalton Trans. (2005) 2842.